Practical Application of Space Mapping Techniques to the Synthesis of CSRR-Based Artificial Transmission Lines

Ana Rodríguez, Jordi Selga, Ferran Martín, and Vicente E. Boria

Abstract Artificial transmission lines based on metamaterial concepts have been attracting increasing interest from the scientific community. The synthesis process of this type of artificial line is typically a complex task, due to the number of design parameters involved and their mutual dependence. Space mapping techniques are revealed to be very useful for automating the synthesis procedure of these kinds of structures. In this chapter, a review of their application to the automated synthesis of microstrip lines loaded with complementary split ring resonators (CSRRs), either with or without series capacitive gaps, will be presented. The most critical points related to the implementation of these space mapping techniques are discussed in detail. Different examples to illustrate and prove the usefulness of this synthesis methodology are presented.

Keywords Aggressive space mapping · Computer aided design (CAD) · Planar microwave circuits · Complementary split resonators · Artificial transmission lines

1 Introduction

Space mapping (SM) techniques and SM-based surrogate (modeling) have been widely used in the design of many microwave components [1], but their application

A. Rodríguez (✉) · V.E. Boria
Departamento de Comunicaciones-iTEAM, Universitat Politècnica de València, 46022 Valencia, Spain
e-mail: amrodri@iteam.upv.es

V.E. Boria
e-mail: vboria@dcom.upv.es

J. Selga · F. Martín
CIMITEC, Departament d'Enginyeria Electrònica, Universitat Autònoma de Barcelona, 08193 Bellaterra, Spain

F. Martín
e-mail: Ferran.Martin@uab.es

V.E. Boria
Aurora Software and Testing S.L., Valencia, Spain

S. Koziel, L. Leifsson (eds.), *Surrogate-Based Modeling and Optimization*,
DOI 10.1007/978-1-4614-7551-4_4,

to the synthesis of artificial transmission lines is still marginal. Metamaterial transmission lines can be a very interesting alternative to conventional lines for many practical microwave devices [2, 3], since more compact solutions (compatible with planar manufacturing processes) with higher degrees of design flexibility can be obtained. Furthermore, metamaterial transmission lines can also provide many other unique properties not achievable with conventional lines, which include negative or low values of permittivity, permeability, and index of refraction, controllable dispersion, and tailored characteristic impedance values [4]. Their commercial impact is still not very relevant, due the complexity of the related synthesis procedures used nowadays. These procedures are mainly based on the engineer's experience with the help of full-wave electromagnetic (EM) simulators and parameter extraction methods. Hence, the motivation of this chapter is to review some promising advances made recently in the field, which can simplify and speed up the process of artificial line synthesis, and that it is hoped will be of interest to the readers.

There are two main approaches for implementing metamaterial transmission lines. One strategy consists in loading a host transmission line with series capacitances and shunt inductances and, as a result, presenting a composite right/left-handed behavior. In order to have propagation, the series and shunt reactances of the equivalent circuit model have to present opposite signs. Depending on the frequency range, either the loading elements (capacity gaps, strips, vias) or the host line will determine the propagation characteristics. The mushroom structure, originally introduced by Sievenpiper et al. [5] and used often in low-profile antennas in order to improve the gain and directivity, is a good example of this strategy, which is usually known as the CL-loaded approach. The CL-loaded term means that the host transmission line is loaded with series capacitances and shunted inductances.

The alternative technique to obtain metamaterial transmission lines consists of etching electrically small (subwavelength) resonators to the host transmission line (TL): this is called the resonant-type approach [6]. All these artificial transmission lines are also identified as composite right/left-handed (CRLH) lines, since they exhibit left-handed (backward) wave propagation at low frequencies and right-handed (forward) wave propagation at high frequencies [7]. Depending on different aspects, such as the kind of resonator, how it is coupled to the line, and the additional elements it is combined with, it is possible to design many different transmission lines [6, 8]. The split ring resonator (SRR) is probably the most widely used common element, and it is basically composed of two concentric metallic rings with splits at their opposite ends [9]. A periodic array of SRRs was used for the first actual demonstration of a negative index refraction medium [10]. Other electrically small (subwavelength) particle elements inspired by the split ring resonator, such as the complementary split ring resonator (CSRR) [11], and the recently proposed use of open particles (i.e., the open split ring resonator (OSRR) and its complementary OCSRR) can be applied as well as the loading elements of a host transmission line [8]. The present chapter focuses on the automated synthesis of CSRR-based resonant-type artificial TLs, but there are works on the direct extension to other loaded lines, too.

The chapter is organized as follows. First, the CSRR-based artificial transmission lines are introduced and explained in detail. Starting from the physical topology of a

single unit cell, the EM behavior, its equivalent circuit, and the related characteristic electrical parameters are obtained in a straightforward way. From a practical point of view, this is very interesting, since this approach, which is based on SM techniques, greatly reduces the computational time related to the optimization process. Next, the implemented aggressive space mapping (ASM) technique is outlined, as well as its application to the automated synthesis of these lines. Finally, some examples illustrating the potential of this SM technique, along with the main conclusions and future directions in this area of research, are briefly discussed.

2 CSRR-Based Artificial Transmission Lines

In this type of artificial transmission line, the CSRRs usually appear etched on the metalized ground plane of the substrate, and the host line is typically implemented in microstrip technology. Other planar configurations are also possible. The first line under study has a simple geometrical topology that has been widely studied in the literature [12, 13]. ASM techniques have proven to be a suitable synthesis tool for these lines, and similar strategies can be extended to more complex topologies. The layout of a single unit cell is depicted in Fig. 1(a); it consists of a microstrip line with a CSRR etched on the ground plane just beneath the conductor strip. The geometrical dimensions are the width of the microstrip line W, the external CSRR radius r_{ext}, the width of the slots c, the distance between them d, and the split of the rings s_{split}. This structure presents a stop-band response, over a narrow band, as shown in Fig. 2(a). One of these unit cells, or some of the cells after cascading, can be practically used to implement a notch (or stop-band) filter [14, 15].

The second type of artificial transmission line considered is called a CSRR-gap-loaded line to make a clear distinction between it and the previous line. In this type, a simple series gap of length s is introduced in the conductor strip line. This gap is centered with respect to the CSRR locations, as illustrated in Fig. 1(b). Among other applications, there are practical applications of this type of artificial transmission line related to dual-band or enhanced bandwidth components. A slightly different version of this line which presents the series gap with a T-shaped geometry is also often used. This geometry allows an increase in the capacitance value for some practical applications [16, 17].

As the size of the loading elements, the CSRRs, is much smaller than the operating wavelength, the response of these two CSRR-based TLs can be accurately described by equivalent lumped circuit models [12, 13] in the region where these elements are operating. In Fig. 1, the equivalent model for each unit cell is presented as a reactive element, since the CSRR is modeled by the parallel tank composed of C_c and L_c. In the first case (Fig. 1(a)), L represents the line inductance and C the coupling capacitance between the line and the CSRR. We note that the ohmic losses of the CSRR could be easily taken into account by just including a parallel resistance in the model [12]. In the second case, L also represents the line inductance, while C and C_g model the gap and the coupling with the transmission line, respectively.

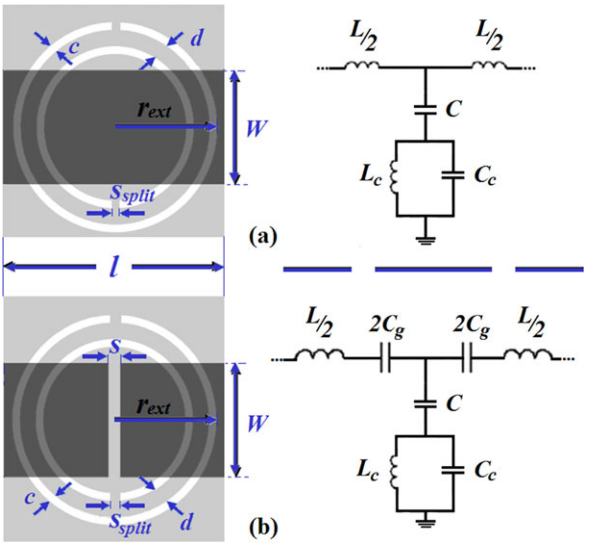

Fig. 1 Layout and equivalent circuit model of a unit cell of a CSRR-loaded line without (**a**) and with (**b**) series gap. The ground plane is depicted in *light gray*

This T-model is achieved after a transformation of the standard π-network [13] that models a series gap in a microstrip line [18]. The values of the circuit elements shown in Fig. 1 can be directly extracted from the EM simulation of these structures (see [12] for the details). The parameter extraction (PE) process is a crucial step in SM techniques, since it directly affects the convergence speed of these algorithms [19]. The agreement between the circuit simulation of the extracted values and the corresponding EM simulation is excellent, as illustrated with the two examples in Fig. 2. The process we have followed is briefly explained for completeness in the following paragraphs.

Two frequencies can be easily identified, by observing Figs. 1 and 2. The frequency that nulls the shunt impedance is represented by f_z, and the one that nulls the shunt admittance is represented by f_0:

$$f_z = \frac{1}{2\pi\sqrt{L_c(C+C_c)}}, \tag{1}$$

$$f_0 = \frac{1}{2\pi\sqrt{L_c C_c}}. \tag{2}$$

The representation of the magnitude of the transmission coefficient, i.e., S_{21}, allows us to identify clearly the transmission zero at f_z. On the other hand, the shunt branch becomes an open circuit for the value of f_0, which causes the reflection coefficient S_{11} to be intercepted with the unit resistance circle in the Smith chart. Moreover, at an angular frequency of $-\pi/2$ ($\pi/2$ for the CSRR-gap-loaded line case), the series and shunt impedances of the T-circuit model of the structure should be equal with opposite signs:

$$Z_s(\omega_{-\pi/2}) = -Z_p(\omega_{-\pi/2}). \tag{3}$$

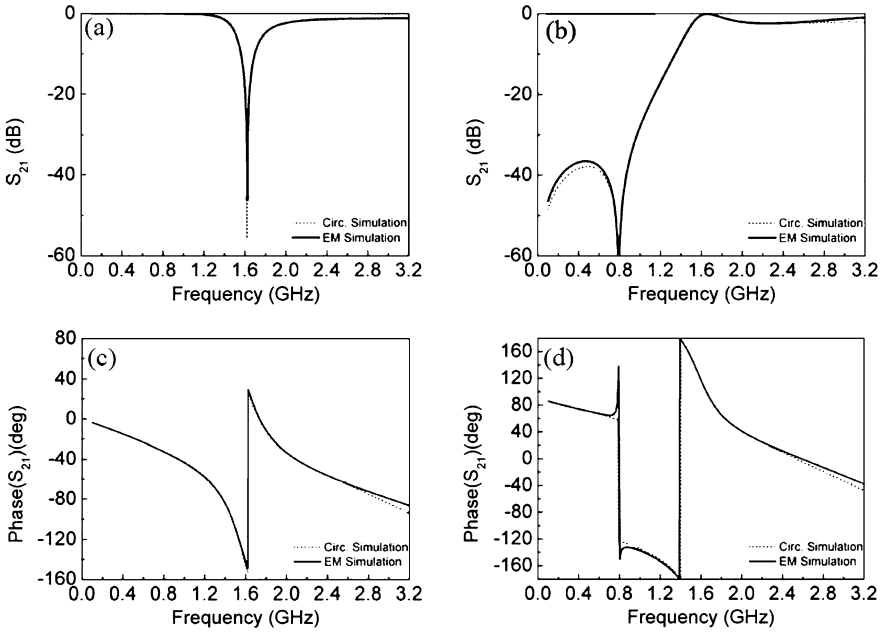

Fig. 2 Typical magnitude and phase of the transmission coefficient of the CSRR-based artificial transmission lines shown in Fig. 1. The plots (**a**) and (**c**) correspond to the CSRR-loaded line; (**b**) and (**d**) to the CSRR-gap-loaded line. EM and electrical simulations are depicted in *bold* and *dotted lines*, respectively

Hence, for the first line all the parameters are determined just by solving the equation system given by the previous expressions. In the CSRR-gap-loaded line, an additional condition is needed to fully determine the complete circuit, which has one more parameter (C_g). This extra condition is given by the resonance frequency of the series branch as follows:

$$f_s = \frac{1}{2\pi\sqrt{LC_g}}, \tag{4}$$

which is simply derived from the interception of S_{11} with the unit conductance circle, when the impedance on the series branch is rendered closed-circuit.

3 Application of SM Techniques

The main advantage of SM techniques is that they shift the optimization load from an expensive "fine" model to a cheaper "coarse" model. In the microwave area, fine models are often based on full-wave EM simulations, while coarse models usually employ equivalent circuits of the structures under study. After a reasonable number of fine model evaluations, SM algorithms lead in general to the construction of a

mapping between "fine" and "coarse" models providing a satisfactory solution in the accurate ("fine") simulation space.

The ASM method was originally introduced by Bandler et al. in 1995 [20]. It is one of the successive enhanced techniques that have been proposed in the literature since the appearance of the first SM approach [21]. In order to automate the synthesis procedure of CSRR-based artificial lines, the constrained version of the Broyden-based linear SM [22] is selected. Our approach uses constraints to avoid the instabilities of the Broyden-based linear SM algorithm, as well as to avoid reaching unwanted (from a practical realization point of view) solutions.

Each SM-based design strategy tries to find a mapping (P), which relates the design parameters of the EM model, denoted from now on as vector $\boldsymbol{x}_{\mathrm{em}}$, and the coarse model parameters, vector $\boldsymbol{x}_c$:

$$\boldsymbol{x}_c = P(\boldsymbol{x}_{\mathrm{em}}) \tag{5}$$

such that the different model responses, $R_{\mathrm{em}}(\boldsymbol{x}_{\mathrm{em}})$ and $R_c(\boldsymbol{x}_c)$, are aligned,

$$R_{\mathrm{em}}(\boldsymbol{x}_{\mathrm{em}}) \approx R_c\big(P(\boldsymbol{x}_{\mathrm{em}})\big), \tag{6}$$

in the region of interest. The solution $\boldsymbol{x}^*_{\mathrm{em}}$ is found via the inverse transformation of P:

$$\boldsymbol{x}^*_{\mathrm{em}} = P^{-1}\big(\boldsymbol{x}^*_c\big), \tag{7}$$

where $\boldsymbol{x}^*_c$ is the optimal coarse solution which provides the desired target response $R_c(\boldsymbol{x}^*_c)$. In the problems we considered, the coarse model parameters are the elements of the corresponding equivalent lumped circuit models. For the EM models, the dielectric characteristic of the substrate and its related thickness are known data, and the geometry dimensions are the design parameters. See Fig. 3 for each of the considered cases. The model response is related to the device behavior, so the scattering parameters are evaluated in a predefined frequency range.

Of course, the goal of ASM is to find the solution $\boldsymbol{x}_{\mathrm{em}}$ which approximates the optimal coarse model response $\boldsymbol{x}^*_c$. This means, expressed in mathematical terms, that we must solve the following set of nonlinear equations:

$$f(\boldsymbol{x}_{\mathrm{em}}) = P(\boldsymbol{x}_{\mathrm{em}}) - \boldsymbol{x}^*_c = 0, \tag{8}$$

where f is a suitable error function. Since ASM is an iterative algorithm, we will add a superscript to the notation in order to indicate the iteration number. Thus, $\boldsymbol{x}^{(j)}_{\mathrm{em}}$ indicates the j-th approximation to the solution layout. The next solution is predicted by applying a step $\boldsymbol{h}^{(j)}$ to the previous one in the quasi-Newton direction,

$$\boldsymbol{x}^{(j+1)}_{\mathrm{em}} = \boldsymbol{x}^{(j)}_{\mathrm{em}} + \boldsymbol{h}^{(j)}, \tag{9}$$

which is calculated as follows:

$$B^{(j)}h^{(j)} = -f^{(j)}, \tag{10}$$

where $\boldsymbol{B}^{(j)}$ is called the Broyden matrix [20, 22], which is properly updated in each iteration. Since the calculation of $\boldsymbol{h}^{(j)}$ requires the inverse of $\boldsymbol{B}^{(j)}$ according to (10), it is more convenient to have the same number of parameters in each model; as a

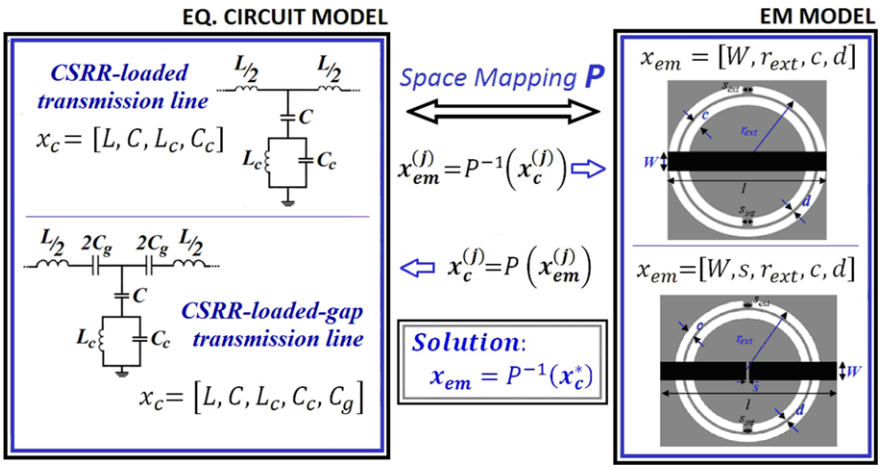

Fig. 3 Conceptual diagram of space mapping techniques for the two cells to be synthesized

result, $\boldsymbol{B}^{(j)}$ is a square, nonsingular matrix. Hence, the split of the CSRR s_{split} is considered a square gap of side c, and the length of the line l is fixed to the diameter value of the CSRR external ring. This is a reasonable assumption due to the fact that larger/smaller lengths of the line would lead to different equivalent circuit models, and on the other hand the CSRR sensitivity on the split size is not very high.

In the constrained approach, $\boldsymbol{h}^{(j)}$ is decreased in the same quasi-Newton direction by a shrinking factor δ, when the new solution $\boldsymbol{x}_{\text{em}}^{(j)}$ is not within the acceptable established limits. Dimensions that are too small may be impossible to implement due to technological limitations. Moreover, the equivalent circuit model used for the PE stage might be inaccurate for very extreme dimensions, which is a critical issue for ASM convergence. The algorithm continues with normal evolution once the quasi-Newton step is properly adjusted; see Fig. 4. Convergence is achieved when the norm of the error function $f^{(j)}$ given by:

$$\left\| f^{(j)} \right\| = \sqrt{\left(L^{(j)} - L^*\right)^2 + \left(C^{(j)} - C^*\right)^2 + \left(L_c^{(j)} - L_c^*\right)^2 + \left(C_c^{(j)} - C_c^*\right)^2} \quad (11)$$

is smaller than a fixed positive value $\eta \ll 1$. In the case of CSRR-gap-loaded lines the stopping criterion is slightly modified to $\| f_{\text{norm}}^{(j)} \| < \eta_1$ and/or $\| f^{(j)} \| < \eta_2$, where the normalized error function is defined as:

$$\left\| f_{\text{norm}}^{(j)} \right\| = \sqrt{\left(1 - \frac{L^{(j)}}{L^*}\right)^2 + \left(1 - \frac{C^{(j)}}{C^*}\right)^2 + \left(1 - \frac{L_c^{(j)}}{L_c^*}\right)^2 + \left(1 - \frac{C_c^{(j)}}{C_c^*}\right)^2} \quad (12)$$

and where η_1, η_2 are small positive numbers close to zero, $\eta_1 < \eta_2 \ll 1$.

For the algorithm initialization, given an ideal target frequency response characterized by $\boldsymbol{x}_c^*$, an initial layout $\boldsymbol{x}_{\text{em}}^{(1)}$ needs to be inferred. This is done by using well-known analytical formulas that link the electrical parameters with the geometrical dimensions of the host line and the CSRR resonator separately, thus not taking

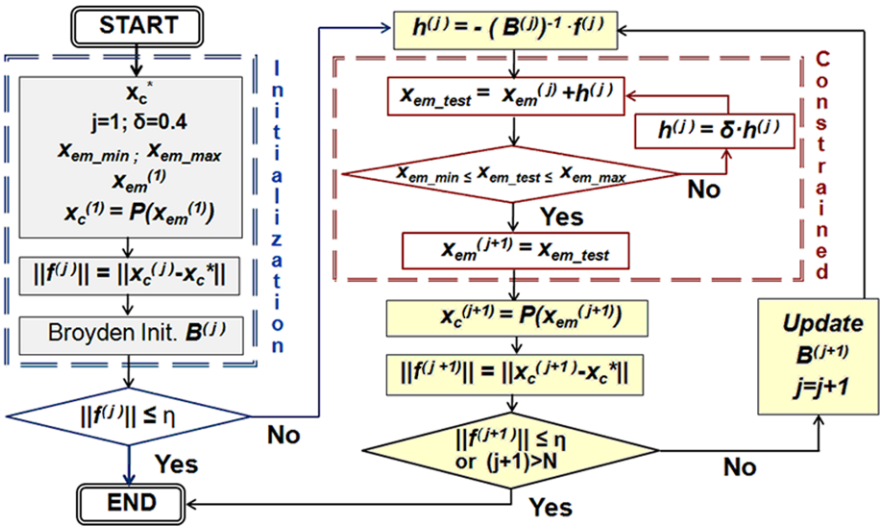

Fig. 4 Flow diagram of the proposed constrained ASM algorithm

into account the coupling between them. For the host line, different models are used depending on the presence or absence of the gap. In the simplest case (i.e., without the gap, see Fig. 1(a)), the characteristic impedance can be approximated by:

$$Z_0 = \sqrt{\frac{L_{\text{pul}}}{C_{\text{pul}}}} \approx \sqrt{\frac{L^*}{C^*}} \tag{13}$$

where L_{pul} and C_{pul} are the per-unit-length inductance and capacitance of the microstrip line, respectively. For a given impedance value and known dielectric constant ε_r, the ratio of the width W over the substrate height h can be calculated as:

$$\frac{W}{d} = \begin{cases} \frac{8e^A}{e^{2A}-2} & \text{for } (W/d) < 2, \\ \frac{2}{\pi}[B - 1 - \ln(2B-1) + \frac{\varepsilon_r - 1}{2\varepsilon_r}\{\ln(B-1) + 0.39 - \frac{0.61}{\varepsilon_r}\}] & \text{for } (W/d) > 2 \end{cases} \tag{14}$$

and hence the initial width is estimated [23]. The terms A and B are given by:

$$\begin{aligned} A &= \frac{Z_0}{60}\sqrt{\frac{\varepsilon_r + 1}{2}} + \frac{\varepsilon_r - 1}{\varepsilon_r + 1}\left(0.23 + \frac{0.11}{\varepsilon_r}\right), \\ B &= \frac{377\pi}{2Z_0\sqrt{\varepsilon_r}}. \end{aligned} \tag{15}$$

A host microstrip line with a gap, according to [18], can be modeled by means of a π-circuit composed of three capacitors (C_s for the series branch and C_p for the parallel capacitance). Those values, depicted in Fig. 5, can be connected with the ones of the π-circuit model in Fig. 1(b) through the following expressions:

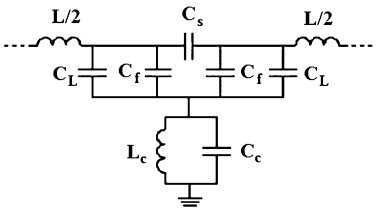

Fig. 5 Equivalent circuit to the simplified model of Fig. 1(b), proposed in [12]

$$C_p = \frac{2C_g^* C^*}{4C_g^* + C^*}, \tag{16}$$

$$C_s = \frac{(2C_g^*)^2}{4C_g^* + C^*}. \tag{17}$$

The parallel capacitance C_p is defined as:

$$C_p = C_f + C_L, \tag{18}$$

where C_L and C_f are the line and the fringing capacitance, respectively. Typically, C_p is dominated by the line capacitance; therefore, we can neglect the fringe capacitance in a first-order approximation, and consider that the parallel capacitance is equal to the line capacitance. Knowing C_L and L^*, the characteristic impedance of the host line is obtained following a similar procedure to (13), and consequently the initial width can also be determined for the line [23].

Now, in order to estimate the CSRR initial dimensions, we need to perform a very simple optimization process. Analytical formulas for the approximate characteristic electrical parameters of a given topology are known (see [24]). In this case, we fix one of the CSRR geometry parameters to a constant value (typically c) to ease the optimization process followed to find a deterministic solution for the initial layout. Therefore, we find the optimal values of r and d that minimize the error function between the electrical parameters of the real structure (L_c, C_c) and the target ones (L_c^*, C_c^*):

$$f_{\text{error}} = \frac{\sqrt{(L_c - L_c^*)^2 + (C_c - C_c^*)^2}}{\sqrt{(L_c^*)^2 + (C_c^*)^2}}. \tag{19}$$

The procedure followed for the initialization of the Broyden matrix $\boldsymbol{B}$ is based on a finite difference scheme. Although the identity matrix is typically chosen for initialization, a different approach was proposed in order to help the algorithm converge faster, considering that the design parameters are completely different in each model, i.e., physical versus electrical ones. To this extent, each geometrical parameter is slightly perturbed from the estimated initial value, the new layout is simulated, and then the corresponding electrical parameters are extracted. Thus, the initial Broyden matrix is calculated as follows:

$$\boldsymbol{B}^{(1)} = \begin{pmatrix} \partial L/\partial W & \partial L/\partial r_{\text{ext}} & \partial L/\partial c & \partial L/\partial d \\ \partial C/\partial W & \partial C/\partial r_{\text{ext}} & \partial C/\partial c & \partial C/\partial d \\ \partial L_c/\partial W & \partial L_c/\partial r_{\text{ext}} & \partial L_c/\partial c & \partial L_c/\partial d \\ \partial C_c/\partial W & \partial C_c/\partial r_{\text{ext}} & \partial C_c/\partial c & \partial C_c/\partial d \end{pmatrix}. \tag{20}$$

To conclude this section, some aspects regarding the practical implementation of the proposed SM method are discussed (further details can be found in [25]). The core of the program (the ASM algorithm) has been implemented in MATLAB [26]. External calls to a microwave engineering CAD suite that allows full-wave simulations are done using scripts. After each layout simulation, MATLAB recovers the control and makes use of the S-parameters to extract the electrical parameters in a straightforward way, as was previously explained. Next, the norm of the error function is evaluated (11)–(12). Normal ASM execution continues if convergence is not reached, or if the maximum number of EM simulations N (established by the user) is not exceeded; see Fig. 4. Thus, a fully automated tool [27–29] that makes it possible to synthesize these artificial transmission lines is available. As a consequence, the design process is shortened from many hours/days to several minutes/hours, and does not require the user to have special designing skills.

4 Validation Examples

In order to demonstrate the capabilities of the proposed synthesis technique, different examples (one for each cell of study) are presented. The optimal coarse solutions for both cases are taken from [12], with the aim of checking whether the proposed synthesis method provides final layouts close enough to the ones already given in [12]. The selected substrate is *Rogers RO3010* with a thickness of $h = 1.27$ mm, a dielectric constant of $\varepsilon_r = 10.2$, and loss tangent $\tan\delta = 0.0023$. Dielectric losses were not taken into account for the EM simulations, and metal parts were considered as perfect conductors (since we did not include a resistance in the equivalent circuit model). For each example we have made use of a different commercial EM solver: *Ansoft Designer* [30] was used in the first case and *Agilent Momentum* [31] in the second one.

4.1 Example of a CSRR-Loaded TL

The optimal target solution $\boldsymbol{x}_c^*$ (see Table 1) has a transmission zero at $f_z = 1$ GHz. The initial layout, $\boldsymbol{x}_{\text{em}}^{(1)}$, is quite shifted from the target response (see Fig. 7), but it can still be considered a good starting point for initiating the algorithm. Nevertheless, it is obvious that a better initial point (smaller value of $\|f^{(1)}\|$) would lead to a faster convergence of the algorithm. In Fig. 6 one can clearly see the evolution of the error function with the execution of the ASM algorithm; it becomes rather small after just ten iterations. The final synthesis was obtained in iteration 17, which means a CPU effort of approximately 30 min (using a standard computer with 3 GB of RAM and a 2.86 GHz clock processor).

A good matching for the responses of the optimal coarse solution $\boldsymbol{x}_c^*$ and the final optimum layout $\boldsymbol{x}_{\text{em}}^*$ can be clearly seen in Fig. 7. The dimensions of the final unit cell are summarized in Table 2, where the initial layout is also included.

Table 1 Coarse solutions and norm of the error function

	L [nH]	C [pF]	L_c [nH]	C_c [nH]	$\|f\|$
Target $\boldsymbol{x}_c^*$	5.080	4.430	2.980	4.060	
Initial $\boldsymbol{x}_c^{(1)}$	8.201	2.793	2.672	4.109	3.5377
Final $\boldsymbol{x}_c^{(17)}$	5.076	4.420	2.986	4.063	0.0124

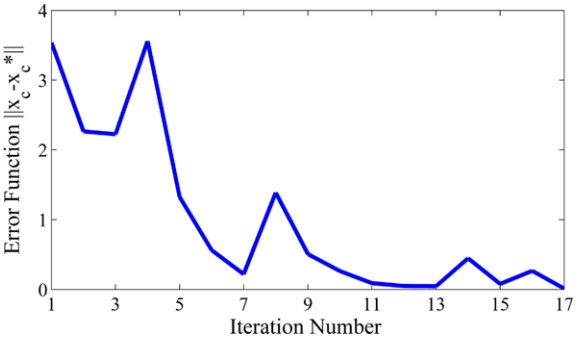

Fig. 6 Evolution of $\|f\|$ versus iteration number for the first example

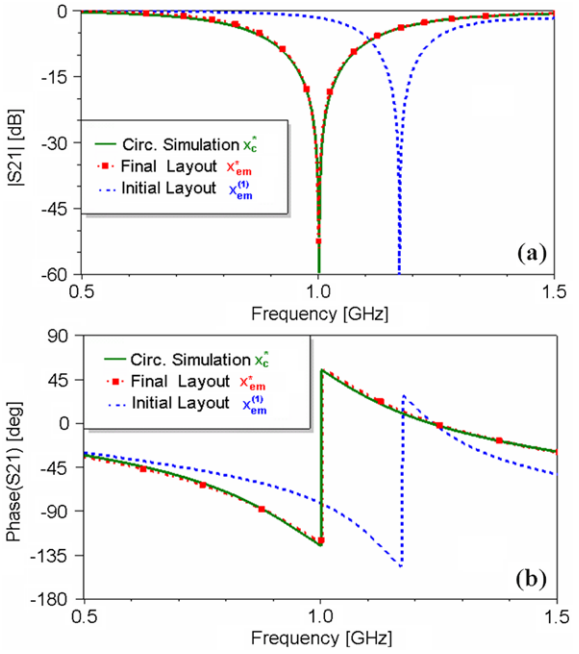

Fig. 7 Magnitude (**a**) and phase (**b**) of transmission coefficient S_{21} at initial solution $\boldsymbol{x}_{\text{em}}^{(1)}$, final solution $\boldsymbol{x}_{\text{em}}^*$, and target circuital solution $\boldsymbol{x}_c^*$

Table 2 Layout dimensions

	r_{ext} [mm]	c [mm]	d [mm]	W [mm]	l_{strip} [mm]
Initial $\boldsymbol{x}_{\text{em}}^{(1)}$	6.39	0.25	0.95	2.43	12.78
Final $\boldsymbol{x}_{\text{em}}^{*}$	5.67	0.33	0.34	4.93	11.34

Table 3 Layout dimensions

	r_{ext} [mm]	c [mm]	d [mm]	W [mm]	s [mm]
Initial $\boldsymbol{x}_{\text{em}}^{(1)}$	5.46	0.25	0.33	1.14	0.11
Final $\boldsymbol{x}_{\text{em}}^{*}$	5.62	0.31	0.19	3.90	0.31

4.2 Example of a CSRR-Gap-Loaded TL

The target parameters of the circuit model for this example are $L^* = 4.92$ nH, $C^* = 35.87$ pF, $L_c^* = 3.41$ nH, $C_c^* = 3.85$ pF, and $C_g^* = 1.05$ pF. Note that the requested value for the coupling capacitance C^* is big due to the presence of the gap, and since its magnitude is much larger than the rest of the circuit parameters, the norm of the normalized error (12) has been used for the stopping criterion. The final synthesis data (see Table 3) were obtained after 25 iterations, which means around 90 min of CPU time, and it can be seen that they are really close to the ones provided in [12] (which were derived via a manual optimization procedure).

The agreement between the circuit simulation of $\boldsymbol{x}_c^*$ and the final EM simulation $\boldsymbol{x}_{\text{em}}^*$ is indeed very good, as it can be see in Fig. 8. There is a slight discrepancy between the measurements and simulations attributed to the tolerances of the fabrication process.

5 Enhancements

In order to increase the robustness and accelerate the convergence rate of the algorithm, some other enhancements have been implemented. For instance, a line search (LS) technique has been introduced in the ASM update stage, with the aim of avoiding abrupt variations in the error norm evolution $\|f\|$ [32]. Introducing LS causes $\|f\|$ to follow a global decreasing behavior until convergence is achieved. See Fig. 9.

When the error function is enormously increased with respect to the previous iteration, taking the full Newton step $\boldsymbol{h}^{(j)}$ is a bad choice. The length of the step is controlled with LS in the same Newton direction by means of a factor λ:

$$\boldsymbol{x}_{\text{em}}^{(j+1)} = \boldsymbol{x}_{\text{em}}^{(j)} + \lambda \cdot \boldsymbol{h}^{(j)}, \quad 0 < \lambda \leq 1. \tag{21}$$

First, λ is chosen equal to unit (i.e., the normal evolution of the algorithm), and if the solution $\boldsymbol{x}_{\text{em}}^{(j+1)}$ does not meet the following criterion:

$$f\left(\boldsymbol{x}_{\text{em}}^{(j+1)}\right) \leq f\left(\boldsymbol{x}_{\text{em}}^{(j)}\right) + \kappa \cdot \nabla f\left(\boldsymbol{x}_{\text{em}}^{(j)}\right) \cdot \lambda \cdot \boldsymbol{h}^{(j)} \quad \text{with } \kappa = 10^{-4}, \tag{22}$$

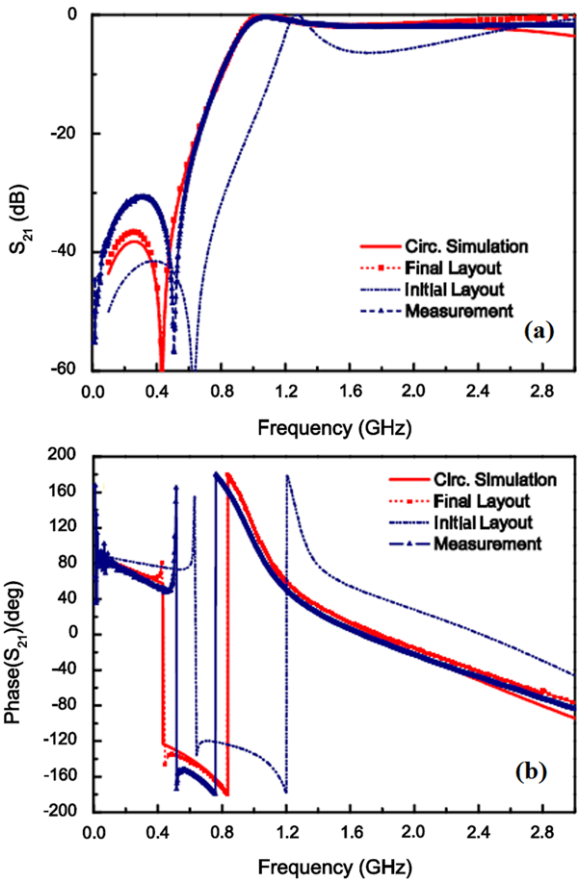

Fig. 8 Magnitude (**a**) and phase (**b**) of the transmission coefficient of the structure previously published in [29]. The initial solution $\boldsymbol{x}_{\text{em}}^{(1)}$, final solution $\boldsymbol{x}_{\text{em}}^{*}$, target response $\boldsymbol{x}_{c}^{*}$, and measurements are drawn with *blue dotted*, *red dotted*, *red solid*, and *solid blue lines*, respectively

several backtracks along the Newton directions are applied until the error function is decreased, or $\boldsymbol{x}_{\text{em}}^{(j+1)}$ is equal to $\boldsymbol{x}_{\text{em}}^{(j)}$. For the first backtrack, the error function is modeled by a quadratic polynomial function, and in the following ones by means of a cubic polynomial approach; see [33] for more details about the LS technique. One example where LS results in a clear improvement is the one shown in Fig. 10. The synthesized cell corresponds to the first type of lines (Fig. 1(a)) with a target response given by $L^{*}[\text{nH}] = 4.860$, $L_c[\text{nH}] = 2.180$, $C^{*}[\text{pF}] = 1.640$, and $C_c^{*}[\text{pF}] = 2.890$. The number of EM simulations needed to find the final synthesis is decreased from 29 to 18, hence reducing the computational time significantly. The initial layout and the corresponding final synthesis dimensions are summarized in Table 4. The ASM constrained approach used a shrinking factor of $\delta = 0.4$.

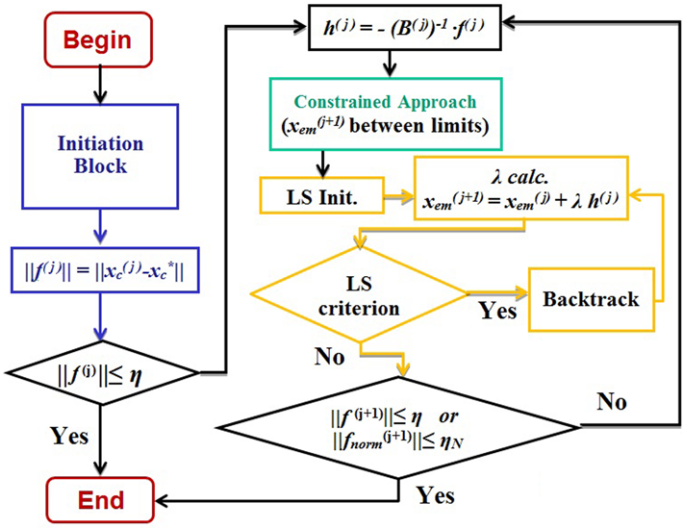

Fig. 9 Flow diagram of the ASM algorithm with the LS technique

Table 4 Layout dimensions and error function values

	r_{ext} [mm]	c [mm]	d [mm]	W [mm]	$\|f\|$
Initial $\boldsymbol{x}_{\text{em}}^{(1)}$	4.83	0.25	0.93	0.99	3.105
ASM $\boldsymbol{x}_{\text{em}}^{*}$ ($\delta = 0.4$)	4.02	0.42	0.15	1.95	0.048
ASM + LS $\boldsymbol{x}_{\text{em}}^{*}$ ($\delta = 0.4$)	4.03	0.43	0.16	1.99	0.050

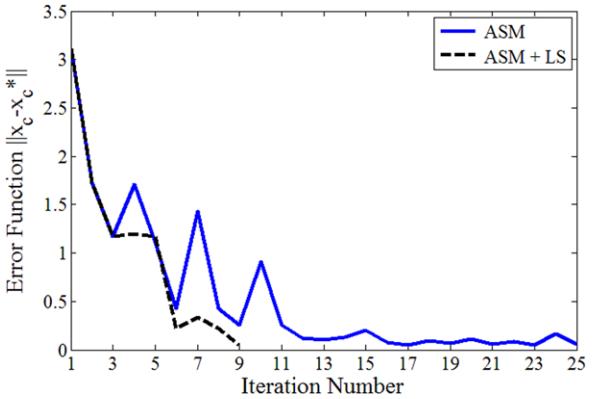

Fig. 10 Evolution of $\|f\|$ versus iteration number, using ASM with $\delta = 0.4$ (*solid blue line*) and ASM + LS (*dashed black line*)

After applying the LS algorithm to several examples, we have found that the introduction of LS does not always provide the expected positive effects. In some cases, we have observed that the convergence of the algorithm with LS can be-

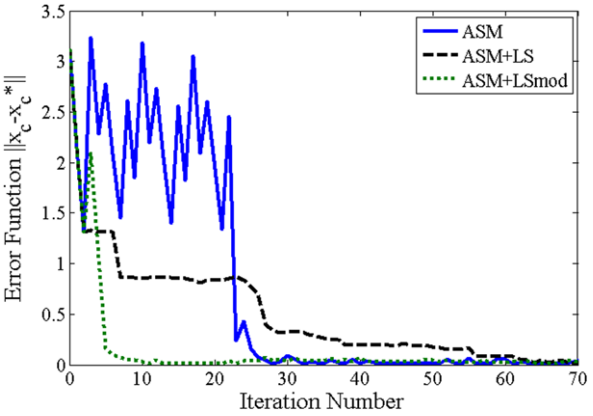

Fig. 11 Evolution of $\|f\|$ versus iteration number, using ASM (*solid blue line*), ASM + LS (*dashed black line*), and ASM + LS modified (*dotted green line*)

Table 5 Layout dimensions and error function values

	r_{ext} [mm]	c [mm]	d [mm]	W [mm]	$\|f\|$
Initial $\boldsymbol{x}_{\text{em}}^{(1)}$	4.83	0.25	0.93	0.99	3.1053
ASM $\boldsymbol{x}_{\text{em}}^{*}$ ($\delta = 0.3$)	4.02	0.40	0.18	1.93	0.0104
ASM + LS $\boldsymbol{x}_{\text{em}}^{*}$ ($\delta = 0.3$)	4.03	0.38	0.19	1.95	0.0137
ASM + LS mod $\boldsymbol{x}_{\text{em}}^{*}$ ($\delta = 0.3$)	4.02	0.40	0.18	1.93	0.0104

come slower than without it. Each backtrack performed implies an additional EM simulation. If the error is high (far from the final synthesis) it has no sense to perform several backtracks when previous iteration presents an error of the same order. Many backtracks will have a high cost and not a real benefit, it is enough to apply a small correction in order not to slow the progress of the algorithm. Therefore, only one backtrack is performed while the norm of the error (or normalized error for the case of CSRR-gap loaded lines) is still far from the stopping criterion for the ASM algorithm. In Fig. 11 this fact is illustrated using the same target response as tested previously but a different shrinking factor: $\delta = 0.3$. The algorithm is forced to continue until 70 iterations to clearly appreciate the softer evolution of the algorithm when standard LS is applied. For the modified LS algorithm, convergence is already achieved at iteration 13, whereas the normal execution of ASM ($\delta = 0.3$) converges at iteration 44. All solutions for this last example are collected in Table 5. It is remarkable that sometimes choosing a bad value of δ can also lead to a slow convergence of the algorithm, and this modified solution of LS can help to minimize that effect.

6 Conclusions

In conclusion, it has been demonstrated that SM techniques are very valuable when used for the automated and efficient synthesis of CSRR-based artificial transmission lines. A robust method, which provides very good agreement between the target response and the EM simulation of the final layout solution, has been successfully proposed. This work opens a promising path towards the application of similar methodologies to synthesize other artificial transmission lines, as well as more complex passive devices based on them.

References

1. Bandler, J.W., Cheng, Q.S., Dakroury, S.A., Mohamed, A.S., Bakr, M.H., Madsen, K., Sondergaard, J.: Space mapping: the state of the art. IEEE Trans. Microw. Theory Tech. (2004). doi:10.1109/TMTT.2003.820904
2. Gil Barba, M.: Resonant-type metamaterial transmission lines and their application to microwave device design. Ph.D. dissertation, Universitat Autònoma de Barcelona (2009)
3. Durán-Sindreu, M.: Miniaturization of planar microwave components based on semi-lumped elements and artificial transmission lines. Ph.D. dissertation, Universitat Autònoma de Barcelona (2011)
4. Eleftheriades, G.V.: EM transmission-line metamaterials. Mater. Today **12**, 30–41 (2009)
5. Sievenpiper, D., Zhang, L., Bross, R.F.J., Alexópolous, N.G., Yablonovitch, E.: High-impedance electromagnetic surface with a forbidden frequency band. IEEE Trans. Microw. Theory Tech. **47**(11), 2059–2074 (1999). doi:10.1109/22.798001
6. Marqués, R., Martín, F., Sorolla, M.: Metamaterials with Negative Parameters: Theory, Design and Microwave Applications. Wiley, New York (2007)
7. Caloz, C., Itoh, T.: Novel microwave devices and structures based on the transmission line approach of meta-materials. Paper presented at IEEE MTT International Microwave Symposium, Philadelphia, PA (USA) (June 2003). doi:10.1109/MWSYM.2003.1210914
8. Durán-Sindreu, M., Aznar, F., Vélez, A., Bonache, J., Martín, F.: Analysis and applications of OSRR- and OCSRR-loaded transmission lines: A new path for the design of compact transmission line metamaterials. Paper presented at 3rd International Congress on Advanced Electromagnetics Materials in Microwaves and Optics, London (UK), Sept. 2009. doi:10.1016/j.bbr.2011.03.031
9. Marqués, R., Martel, J., Mesa, F., Medina, F.: Left-handed-media simulation and transmission of EM waves in subwavelength split-ring-resonator-loaded metallic waveguides. Phys. Rev. Lett. **89**(18) (2002). doi:10.1103/PhysRevLett.89.183901
10. Pendry, J.B., Holden, A.J., Robbins, D.J., Stewart, W.J.: Magnetism from conductors and enhanced nonlinear phenomena. IEEE Trans. Microw. Theory Tech. **47**(11), 2075–2084 (1999). doi:10.1109/22.798002
11. Falcone, F., Lopetegi, T., Laso, M.A.G., Baena, J.D., Bonache, J., Beruete, M., Marqués, R., Martín, F., Sorolla, M.: Babinet principle applied to the design of metasurfaces and metamaterials. Phys. Rev. Lett. **93**(4) (2004). doi:10.1103/PhysRevLett.93.197401
12. Bonache, J., Gil, M., Gil, I., Garcia-García, J., Martín, F.: On the electrical characteristics of complementary metamaterial resonators. IEEE Microw. Wirel. Compon. Lett. **16**(10), 543–545 (2006). doi:10.1109/LMWC.2006.882400
13. Bonache, J., Gil, M., Gil, I., Garcia-García, J., Martín, F.: Parametric analysis of microstrip lines loaded with complementary split ring resonators. Microw. Opt. Technol. Lett. **50**, 2093–2096 (2008). doi:10.1002/mop.23571
14. Falcone, F., Lopetegi, T., Baena, J.D., Marqués, R., Martín, F., Sorolla, M.: Effective negative-ε stopband microstrip lines based on complementary split ring resonators. IEEE Microw. Wirel. Compon. Lett. **14**(6), 280–282 (2004). doi:10.1109/LMWC.2004.828029

15. Kshetrimayum, K.S., Kallapudi, S., Karthikeyan, S.S.: Stop band characteristics for periodic patterns of CSRRs in the ground plane. IETE Tech. Rev. **24**(6), 449–460 (2007)
16. Bonache, J., Siso, G., Gil, M., Martín, F.: Dispersion engineering in resonant type metamaterial transmission lines and applications. In: Zouhdi, S. (ed.) Metamaterials and Plasmonics: Fundamentals, Modelling, Applications, pp. 269–276. Springer, New York (2009)
17. Siso, G., Bonache, J., Martín, F.: Miniaturization and dual-band operation in planar microwave components by using resonant-type metamaterial transmission lines. Paper presented at IEEE MTT-S International Microwave Workshop Series (IMWS 2008). Chengdu (China). doi:10.1109/IMWS.2008.4782255
18. Gupta, K.C., Garg, R., Bahl, I., Bhartia, P.: Microstrip Lines and Slotlines, 2nd edn. Artech House Microwave Library (1996)
19. Bakr, M.H., Bandler, J.W., Georgieva, N., Madsen, K.: A hybrid aggressive space-mapping algorithm for EM optimization. IEEE Trans. Microw. Theory Tech. **47**(12), 2440–2449 (1999). doi:10.1109/22.808991
20. Bandler, J.W., Biernacki, R.M., Chen, S.H., Hemmers, R.H., Madsen, K.: Electromagnetic optimization exploiting aggressive space mapping. IEEE Trans. Microw. Theory Tech. **43**(12), 2874–2882 (1995). doi:10.1109/22.475649
21. Bandler, J.W., Biernacki, R.M., Chen, S.H., Grobelny, P.A., Hemmers, R.H.: Space mapping technique for electromagnetic optimization. IEEE Trans. Microw. Theory Tech. **42**(12), 2536–2544 (1994). doi:10.1109/22.339794
22. Rayas-Sanchez, J.E., Gutierrez-Ayala, V.: EM-based Monte Carlo analysis and yield prediction of microwave circuits using linear-input neural-output space mapping. IEEE Trans. Microw. Theory Tech. **54**(12), 4528–4537 (2006). doi:10.1109/TMTT.2006.885902
23. Pozar, D.M.: Microwave Engineering, 3rd edn. Wiley, New York (2005)
24. Baena, J.D., Bonache, J., Martín, F., Marqués, R., Falcone, F., Lopetegi, I., Laso, M.A.G., García, J., Gil, I., Flores, M., Sorolla, M.: Equivalent circuit models for split ring resonators and complementary split ring resonators coupled to planar transmission lines. IEEE Trans. Microw. Theory Tech. **53**(4), 1451–1461 (2005). doi:10.1109/TMTT.2005.845211
25. Selga, J., Rodríguez, A., Gil, M., Carbonell, J., Boria, V.E., Martín, F.: Synthesis of planar microwave circuits through aggressive space mapping using commercially available software packages. Int. J. RF Microw. Comput.-Aided Eng. **20**, 527–534 (2010). doi:10.1002/mmce.20458
26. MATLAB version 2010a, The MathWorks Inc., Natick, MA (2010)
27. Rodriguez, A., Selga, J., Gil, M., Carbonell, J., Boria, V.E., Martin, F.: Automated synthesis of resonant-type metamaterial transmission lines using aggressive space mapping. In: Microwave Symposium Digest (MTT), 2010 IEEE MTT-S International, 23–28 May, pp. 209–212 (2010). doi:10.1109/MWSYM.2010.5517444
28. Selga, J., Rodriguez, A., Gil, M., Carbonell, J., Boria, V.E., Martín, F.: Towards the automatic layout synthesis in resonant-type metamaterial transmission lines. IET Microw. Antennas Propag. **4**(8), 1007–1015 (2010). doi:10.1049/iet-map.2009.0551
29. Selga, J., Rodriguez, A., Boria, V.E., Martin, F.: Application of aggressive space mapping to the synthesis of composite right/left handed (CRLH) transmission lines based on complementary split ring resonators (CSRRs). In: 2011 41st European Microwave Conference (EuMC), 10–13 Oct., pp. 968–971 (2011)
30. Ansoft Designer version 6.1.0. Ansys Inc., Canonsburg, PA (2010)
31. Agilent Momentum version 8.20.374. Agilent Technologies, Santa Clara, CA (2008)
32. Rodríguez, A., Selga, J., Martín, F., Boria, V.E.: On the implementation of a robust algorithm which automates the synthesis of artificial transmission lines based on CSRRs. In: Proceedings of International Congress on Advanced Electromagnetic Materials in Microwaves and Optics, Barcelona, Spain, Oct. (2011)
33. Press, W.H., Teukolsky, S.A., Vetterling, W.T., Flannery, B.P.: Numerical Recipes in C: The Art of Scientific Computing, 2nd edn. Cambridge University Press, Cambridge (1992)